

Motion compensated renal diffusion weighted imaging

Sean McTavish¹ | Anh T. Van¹ | Johannes M. Peeters² | Kilian Weiss³ |
Marcus R. Makowski¹ | Rickmer F. Braren¹ | Dimitrios C. Karampinos¹

¹Department of Diagnostic and Interventional Radiology, School of Medicine, Technical University of Munich, Munich, Germany

²Philips Healthcare, Best, the Netherlands

³Philips Healthcare, Hamburg, Germany

Correspondence

Sean McTavish, Department of Diagnostic and Interventional Radiology, School of Medicine, Klinikum Rechts der Isar, Technical University of Munich, Ismaninger Str. 22, 81675 Munich, Germany, telephone: +49 89 4140-7302
Email: sean.mctavish@tum.de

Funding information

Philips Healthcare; Philips

Purpose: To assess the effect of respiratory motion and cardiac driven pulsation in renal DWI and to examine asymmetrical velocity-compensated diffusion encoding waveforms for robust ADC mapping in the kidneys.

Methods: The standard monopolar Stejskal-Tanner pulsed gradient spin echo (pgse) and the asymmetric bipolar velocity-compensated (asym-vc) diffusion encoding waveforms were used for coronal renal DWI at 3T. The robustness of the ADC quantification in the kidneys was tested with the aforementioned waveforms in respiratory-triggered and breath-held cardiac-triggered scans at different trigger delays in 10 healthy subjects.

Results: The pgse waveform showed higher ADC values in the right kidney at short trigger delays in comparison to longer trigger delays in the respiratory triggered scans when the diffusion gradient was applied in the feet-head (FH) direction. The coefficient of variation over all respiratory trigger delays, averaged over all subjects was 0.15 for the pgse waveform in the right kidney when diffusion was measured in the FH direction; the corresponding coefficient of variation for the asym-vc waveform was 0.06. The effect of cardiac driven pulsation was found to be small in comparison to the effect of respiratory motion.

Conclusion: Short trigger delays in respiratory-triggered scans can cause higher ADC values in comparison to longer trigger delays in renal DWI, especially in the right kidney when diffusion is measured in the FH direction. The asym-vc waveform can reduce ADC variation due to respiratory motion in respiratory-triggered scans at the cost of reduced SNR compared to the pgse waveform.

KEYWORDS

ADC mapping, diffusion-weighted imaging, kidney imaging, motion compensation, renal imaging, velocity compensated diffusion waveforms

1 | INTRODUCTION

Diffusion-weighted imaging (DWI) has been gaining attention in renal imaging and apparent diffusion

coefficient (ADC) mapping has been proposed as a potential biomarker for the assessment of renal fibrosis in chronic kidney disease and renal carcinoma [1–6].

Consensus-based technical recommendations have recently been summarized for clinical translation of renal DWI, proposing a respiratory triggered or gated acquisition to mitigate respiratory motion effects [7]. However, there are only limited studies investigating the impact of physiological motion on renal DWI [8–13].

The traditional Stejskal-Tanner pulsed gradient spin echo (pgse) diffusion encoding waveform has two trapezoidal gradients of equal strength and duration on either side of a refocusing pulse in a spin echo sequence [14]. Random motion of spins during the diffusion encoding period causes spin phase dispersion and subsequently signal loss, which is the basis of the diffusion contrast. However, sources of motion that are not due to the random motion of spins, such as respiratory motion, cardiovascular motion, peristaltic motion, or involuntary bulk motion of the subject may also cause intravoxel dephasing and therefore signal loss, thereby confounding the obtained diffusion-weighted images and estimated diffusion parameters. If the motion is severe enough, it is possible that complete intravoxel dephasing will occur, causing the measured signal to be at the noise floor and the diffusion coefficient to be erroneously measured to be much greater than that of the free diffusion of water. DWI in the abdomen is especially susceptible to respiratory and cardiovascular motion due to the close proximity of the heart, lungs, and large pulsating vessels. Coronal slices have the advantage that they can more easily provide full kidney coverage than axial slices, but they can be susceptible to in-plane motion artifacts [15].

Respiratory-triggered scans are typically used to overcome subject respiratory motion both in the kidneys [1–6,8,9,13,16–18] and other organs such as the liver [19–24]. Cardiac-triggered scans have also been proposed to overcome motion artifacts caused by cardiac driven pulsation [22,25–27]. However, the low efficiency of simultaneous respiratory and cardiac-triggered DWI scans can make cardiac triggering impractical in a clinical setting. Furthermore, it has been suggested that renal blood flow is pulsatile and depends on the cardiac cycle, which affects the perfusion fraction [13] and, therefore, renal ADC values when low b -values are used [8,10,12]. In the literature, there is a large variation of reported ADC values in renal DWI, both between subjects and between studies, which could be due to factors such as physiological variation, the effect of perfusion signal or the choice of b -values [3], but can also be attributed in part to physiological motion.

Motion-compensated diffusion encoding gradient waveforms have recently been proposed as alternatives to overcome the effects of motion in DWI of other organs such as the heart [28–32], the liver [27,28,33–39], and the pancreas [40]. A symmetric bipolar velocity

compensated waveform (sym-vc) can be designed such that the gradient first moment ($m_1 = \gamma \int tG(t)dt$) is equal to zero, meaning that spins which move with a constant velocity accumulate no extra phase and therefore no signal is lost. The sym-vc waveform is not optimal in terms of TE as there is a deadtime between the excitation and refocusing pulses that is not used for diffusion encoding when an EPI readout is used. Several different motion compensated diffusion encoding waveforms that use an asymmetric design for TE optimization have been proposed [28,29,33–39,41–44]. A formulation was recently introduced for the on-the-scanner computation of a near TE-optimal motion-compensated diffusion waveform with concomitant field correction, labeled as the asymmetric velocity compensated diffusion encoding waveform (asym-vc), which allows for flexibility in DWI protocol optimization [35].

The purpose of this work is to assess the effect of respiratory and cardiac driven pulsation in renal DWI and to evaluate the near TE-optimal asymmetrical velocity compensated diffusion encoding asym-vc waveform in the context of coronal ADC mapping in the kidney.

2 | METHODS

2.1 | MRI measurements

MRI measurements were performed in 10 healthy volunteers (mean age, 30 ± 5 y) on a 3 T Ingenia Elition X scanner (Philips Healthcare, Best, Netherlands), with a maximum gradient amplitude of 45 mT/m and a maximum slew rate of 220 T/m/s. The built in 12-channel posterior and 16-channel anterior coil were used for signal reception. The study was approved by the local ethics commission and all volunteers consented for their participation in the study.

Breath-held cardiac triggered scans, respiratory triggered dynamic scans and respiratory triggered ADC measurements using both pgse and asym-vc diffusion encoding waveforms were carried out in subsets of the 10 total volunteers. All DWI was carried out in the coronal plane using a single-shot echo planar readout with a FOV of 240×312 mm², an in-plane resolution of 2.5×2.5 mm², a slice thickness of between 6 and 12 mm, depending on the individual acquisition, a parallel imaging SENSE factor of $R = 3$ in the left–right (LR) direction and a bandwidth in the phase-encoding direction of between 42.3 Hz/pixel and 49.8 Hz/pixel. Since partial Fourier encoding can increase the sensitivity to motion due to its reduced k -space coverage [45,46], no partial Fourier encoding was used. The TEs of the pgse and asym-vc diffusion encoding waveforms were 64 ms and 92 ms, respectively, for a maximum

b -value of 600 s/mm². The velocity-compensated asym-vc waveform had an $m_1 = \int tG(t)dt = 0$, and had a concomitant field corrected near TE-optimal asymmetrical design [34,35]. Where applicable, ADC values were calculated using a monoexponential fit. A respiratory belt was used to track respiratory motion.

2.2 | Breath-held cardiac triggered measurements and analysis

For a subset of 4 out of the 10 healthy volunteers, breath-held cardiac triggered scans were performed to assess cardiovascular motion effects. An electrocardiogram (ECG) signal was used to perform cardiac triggering. Breath holds were done in end-expiration. A single coronal slice covering both kidneys was scanned with both the pgse and asym-vc diffusion encoding waveforms, with a 6 mm slice thickness and b -values of [100, 600] s/mm² using corresponding repetitions of [2,3] per diffusion encoding direction. Diffusion encoding was applied in the feet-head (FH), left-right (LR), and anterior-posterior (AP) directions in separate scans within the same examination. Cardiac trigger delays of 21 ms (shortest), mid diastole and end diastole were used in separate scans. The mid diastole and end diastole were determined for each subject in the scanner software using the subject's heart rate before the beginning of the scan. Each acquisition was performed on every second heartbeat and the TR was therefore dependent on the cardiac cycle of each subject, giving a total breath hold time of approximately 10 s per scan.

Region of interest (ROI) drawing was performed on the pgse $b = 100$ s/mm² image at the cardiac end diastole trigger delay, which had been averaged over all repetitions in the FH diffusion direction. Five ROIs were drawn per kidney mainly in the cortex and these ROIs were propagated through the ADC maps for all diffusion directions, trigger delays, and diffusion encoding waveforms. Small adjustments were made if an ROI was no longer in the cortex. The ADC was calculated per diffusion direction from the two acquired b -values of [100, 600] s/mm² after averaging per b -value.

At each cardiac trigger delay, the statistics for characterizing the variation along the subject dimension, the mean ADC over all subjects, $ADC_{\text{mean_subjects}}$, and the SD of the mean ADC over all subjects, $ADC_{\text{SD_subjects}}$, were computed separately for each kidney. In each subject, the mean ADC over cardiac trigger delays, $ADC_{\text{mean_tds}}$, the SD of the ADC over cardiac trigger delays, $ADC_{\text{SD_tds}}$, and the coefficient of variation across cardiac trigger delays CV_{tds} were also computed for characterizing the variation along the cardiac trigger delay dimension separately for each kidney.

A global $CV_{\text{tds_global}}$ was finally determined by taking the RMS average over all subjects, from the equation [47]:

$$CV_{\text{tds_global}} = \frac{\sqrt{\sum_{j=1}^m \frac{ADC_{\text{SD_tds}_j}^2}{m}}}{\sum_{j=1}^m \frac{ADC_{\text{mean_tds}_j}}{m}}, \quad (1)$$

where m is the number of subjects, $ADC_{\text{SD_tds}_j}$ is the SD of ADC across trigger delays for subject j and $ADC_{\text{mean_tds}_j}$ is the mean ADC across delays for subject j . The global $ADC_{\text{SD_tds_global}}$ s were found from the RMS average over all subjects, and the global $ADC_{\text{mean_tds_global}}$ s were found from averaging over all subjects.

2.3 | Free breathing real time scan measurement

A free breathing real time scan was performed in a single subject to visually assess the degree of translation of the kidneys due to respiration using a real time turbo field echo (TFE) sequence. The balanced TFE acquisition used a TR/TE = 2.4/1.18 ms.

2.4 | Respiratory triggered dynamic scan measurements and analysis

For a different subset of 4 out of the 10 healthy volunteers, respiratory triggered dynamic scans were performed in a single coronal slice with 20 dynamics (i.e. repetitions), a slice thickness of 12 mm and a b -value of 600 s/mm² with both the pgse and asym-vc diffusion waveforms. Although a slice thickness of 12 mm is very thick for kidney DWI, this thickness was chosen to increase the effect of intravoxel dephasing and to therefore clearly demonstrate the effect of motion on signal loss. Separate scans with diffusion encoding in the FH, LR, and AP directions was performed. For each diffusion encoding direction, respiratory trigger delays of 100, 400, and 800 ms from the beginning of the expiration period were used, corresponding approximately to the beginning, middle and end of the expiration period. The TR was determined by the breathing cycle of each volunteer and was in the range of approximately 3000–6000 ms. Five ROIs were drawn per slice per kidney mainly in the cortex. ROI drawing was performed on a pgse $b = 600$ s/mm² image at a respiratory trigger delay of 100 ms that was averaged over all dynamics, and these ROIs were propagated through all dynamics, trigger delays, and diffusion encoding waveforms. Separate ROIs were drawn per diffusion encoding direction. Small adjustments were made if an ROI

was no longer in the cortex. Each ROI was propagated through all dynamics for a particular scan and no adjustments were made for individual dynamics. The average DW signal value was estimated from the average of the five ROIs and the coefficient of variation across dynamics, CV_{dyn} , was determined to assess the variability of the DW signal.

2.5 | Respiratory triggered ADC mapping measurements and analysis

For each of the 10 healthy volunteers, three slices covering both kidneys were acquired in the coronal plane with a slice thickness of 6 mm, a slice gap of 2 mm, b -values of [100, 600] s/mm^2 , and corresponding repetitions of [2,3] per diffusion encoding direction. Diffusion encoding was applied in the FH, LR and AP directions. Both the pgse and asym-vc diffusion encoding waveforms were used in separate scans within the same examination. Respiratory trigger delays of 100, 400, and 800 ms were used. The TR was determined by the breathing cycle of each volunteer and was in the range of approximately 3000–6000 ms.

Five ROIs were drawn per slice per kidney mainly in the cortex. The ROI drawing was performed on the pgse $b = 100 s/mm^2$ image at a respiratory trigger delay of 100 ms which had been averaged over all diffusion encoding directions, and these ROIs were propagated through the ADC maps for all diffusion directions, trigger delays, and diffusion encoding waveforms. Small adjustments were made if an ROI was no longer in the cortex. The ADC map was calculated from the two acquired b -values, and the ADC values per slice were found from the average of the ADC values of each ROI.

At each respiratory delay (100, 400, and 800 ms), the $ADC_{\text{mean_subjects}}$ and the $ADC_{SD_subjects}$ statistics for characterizing the variation along the subject dimension were computed separately for each kidney. For each subject, the $ADC_{\text{mean_tds}}$, the ADC_{SD_tds} and the coefficient of variation across respiratory trigger delays CV_{tds} were also computed for characterizing the variation along the respiratory trigger delay dimension separately for each kidney. A global $CV_{\text{tds_global}}$ was finally determined by taking an RMS average over all subjects following equation 1. The global $ADC_{SD_tds_global}$ s were found from the RMS average over all subjects, and the global $ADC_{\text{mean_tds_global}}$ s were found from averaging over all subjects.

To assess the effect of different breathing patterns on the ADC value, three further respiratory triggered scans with identical scan parameters and using the same ROI analysis were performed in a single subject. The subject was instructed to use three different breathing

patterns – deep breathing, medium breathing, and shallow breathing.

2.6 | SNR mapping scan measurements and simulation

To measure the apparent SNR and the impact of the increased TE of the asym-vc waveform in comparison to the pgse waveform, further respiratory triggered dynamic scans were performed in a single subject with both the pgse and asym-vc diffusion waveforms. Further information is given in the Supporting Information Materials, which are available online.

3 | RESULTS

3.1 | Breath-held cardiac triggered results

Figure 1 shows ADC maps of measurements using the pgse and asym-vc waveforms at different cardiac trigger delays for one volunteer. There were no large differences in ADC between the trigger delays for either waveform in either kidney. In the superior pole of the left kidney for the pgse waveform, there was a small increase in ADC between the shortest cardiac trigger delay and the other two cardiac trigger delays in the volunteer shown. The asym-vc waveform gave an ADC map with lower SNR due to the prolonged TE.

Table 1 shows the $ADC_{\text{mean_subjects}}$, $ADC_{\text{mean_tds_global}}$, $ADC_{SD_subjects}$, $ADC_{SD_tds_global}$ and $CV_{\text{tds_global}}$ over all subjects for both kidneys. In both kidneys, the $ADC_{\text{mean_subjects}}$ s were slightly higher for the asym-vc waveform compared to the pgse waveform for all diffusion directions. In the left kidney for the pgse waveform, in all diffusion directions the $ADC_{\text{mean_subjects}}$ was smallest at the shortest cardiac trigger delay compared to the mid diastole and end diastole cardiac trigger delays, which was not the case for the asym-vc waveform. In both kidneys, the $ADC_{SD_subjects}$ s were similar between the two waveforms for all diffusion directions and no systematic differences were observed. In the right kidney, the $CV_{\text{tds_global}}$ s were similar between pgse and asym-vc for all diffusion directions and were below or equal to 0.05 in all cases. In the left kidney, the $CV_{\text{tds_global}}$ s were similar between pgse and asym-vc for the FH and AP diffusion directions and all were below or equal to 0.06, but increased for the asym-vc waveform and LR diffusion direction. The ADC_{mean} results for the breath-held cardiac triggered experiments for all subjects are shown in the Supporting Information Figure S1.

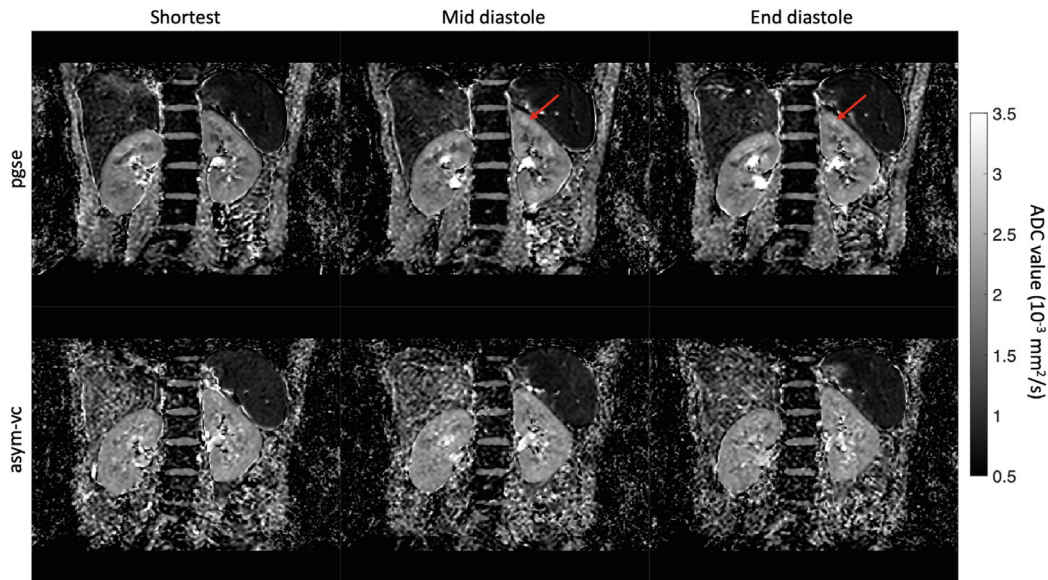


Figure 1 ADC maps of the pgse and asym-vc waveforms at different cardiac trigger delays, with diffusion measured in the FH direction. There do not appear to be any large differences in ADC between the trigger delays for either waveform in either kidney. In the superior pole of the left kidney for the pgse waveform, there is a small increase in ADC (highlighted by the arrows) between the shortest cardiac trigger delay and the other two cardiac trigger delays in the volunteer shown. The asym-vc waveform gives an ADC map with lower SNR due to the prolonged TE

3.2 | Free breathing dynamic scan results

Figure 2 shows a real time imaging balanced TFE sequence of the kidneys in the coronal plane in a free breathing scan. It can be seen that both kidneys move significantly as a result of respiratory motion.

3.3 | Respiratory triggered dynamic scan results

Figure 3 shows diffusion weighted dynamic images of the kidney for one volunteer acquired with the pgse diffusion encoding waveform applied along the FH direction and respiratory triggering with a respiratory trigger delay of 100 ms. In dynamics 1,4,5, and 6, the right kidney shows a large amount of signal loss as a result of intravoxel dephasing due to motion. The left kidney also shows significant signal loss in dynamic 6, and partial signal loss in dynamic 4, but is overall not as severely affected by motion as the right kidney.

Figure 4 shows the results from the respiratory triggered dynamic scans for diffusion in the FH direction for one subject. In the right kidney, at trigger delays of 100 and 400 ms in particular, there were many dynamics for which the pgse waveform exhibited a large amount of signal loss. The CV_{dyn} s for the pgse waveform in the right kidney were 0.55, 0.51, and 0.51 for the respiratory trigger delays of 100,

400, and 800 ms, respectively. The CV_{dyn} s for the asym-vc waveform in the right kidney were 0.16, 0.15, and 0.11 for the respiratory trigger delays of 100, 400, and 800 ms, respectively, which showed a large decrease in CV_{dyn} for all respiratory trigger delays compared to pgse. The CV_{dyn} s for the pgse waveform in the left kidney were 0.24, 0.33, and 0.26 for the respiratory trigger delays of 100, 400, and 800 ms, respectively. The CV_{dyn} s for the asym-vc waveform in the left kidney were 0.21, 0.22, and 0.17 for the respiratory trigger delays of 100, 400, and 800 ms, respectively, which again showed a decrease in CV_{dyn} for all respiratory trigger delays compared to pgse, but not as large of a decrease in CV_{dyn} as in the right kidney.

Figure 5 shows the CV_{dyn} s from the respiratory triggered dynamic scans for all volunteers and all diffusion directions. In general, the largest differences between the CV_{dyn} s of pgse and asym-vc were in the right kidney in the FH diffusion direction, especially at the shortest respiratory trigger delay of 100 ms. pgse also typically had larger CV_{dyn} s than asym-vc in the left kidney in the FH diffusion direction, but the differences were not as large as in the right kidney. The FH direction is the direction in which the kidney is expected to move the most during respiration. In all subjects, pgse had a larger CV_{dyn} than asym-vc in the left kidney in the LR diffusion direction at a respiratory trigger delay of 100 ms. In the right kidney in the LR diffusion direction, pgse also typically had a larger CV_{dyn} than asym-vc. Both waveforms had a similar CV_{dyn} in the AP diffusion direction.

Table 1 ADC_{mean_subjects}, ADC_{mean_tds_global}, ADC_{SD_subjects}, ADC_{SD_tds_global}, and CV_{tds_global} over all subjects for both kidneys and all diffusion directions across cardiac trigger delays

Kidney	Waveform	Trigger Delay	Diffusion Direction		
			FH	LR	
Right kidney	pgse	Shortest	ADC _{mean_subjects} ±	ADC _{mean_subjects} ±	AP
			ADC _{SD_subjects} (10 ⁻³ mm ² /s)	ADC _{SD_subjects} (10 ⁻³ mm ² /s)	ADC _{mean_subjects} ±
			1.92 ± 0.10	1.94 ± 0.22	ADC _{SD_subjects} (10 ⁻³ mm ² /s)
			2.05 ± 0.11	2.03 ± 0.08	1.82 ± 0.09
			2.00 ± 0.12	2.04 ± 0.08	1.93 ± 0.13
			2.07 ± 0.09	2.04 ± 0.10	1.88 ± 0.10
	asym-vc	Mid diastole	2.18 ± 0.12	2.15 ± 0.07	2.02 ± 0.08
			2.15 ± 0.10	2.07 ± 0.10	2.06 ± 0.13
			ADC _{mean_tds_global} ±	ADC _{mean_tds_global} ±	2.07 ± 0.10
			ADC _{SD_tds_global} (10 ⁻³ mm ² /s)	ADC _{SD_tds_global} (10 ⁻³ mm ² /s)	CV _{tds_global}
			1.99 ± 0.09	2.00 ± 0.10	ADC _{mean_tds_global} ±
			2.13 ± 0.09	2.09 ± 0.10	ADC _{SD_tds_global} (10 ⁻³ mm ² /s)
pgse	All tds	0.05	0.05	1.87 ± 0.06	
		0.04	0.05	2.05 ± 0.06	
asym-vc	All tds	0.04	0.05	0.03	
		0.04	0.05	0.03	
Left Kidney	pgse	Shortest	ADC _{mean_subjects} ±	ADC _{mean_subjects} ±	AP
			ADC _{SD_subjects} (10 ⁻³ mm ² /s)	ADC _{SD_subjects} (10 ⁻³ mm ² /s)	ADC _{mean_subjects} ±
			1.90 ± 0.12	1.97 ± 0.18	ADC _{SD_subjects} (10 ⁻³ mm ² /s)
			2.00 ± 0.06	2.03 ± 0.12	1.75 ± 0.19
			1.99 ± 0.07	2.05 ± 0.13	1.85 ± 0.16
			2.07 ± 0.11	2.16 ± 0.21	1.86 ± 0.18
	asym-vc	Mid diastole	2.14 ± 0.04	2.21 ± 0.09	2.04 ± 0.10
			2.03 ± 0.15	2.10 ± 0.20	2.04 ± 0.17
			ADC _{mean_tds_global} ±	ADC _{mean_tds_global} ±	1.99 ± 0.07
			ADC _{SD_tds_global} (10 ⁻³ mm ² /s)	ADC _{SD_tds_global} (10 ⁻³ mm ² /s)	CV _{tds_global}
			1.96 ± 0.08	2.02 ± 0.07	ADC _{mean_tds_global} ±
			2.08 ± 0.08	2.16 ± 0.15	ADC _{SD_tds_global} (10 ⁻³ mm ² /s)
pgse	All tds	0.04	0.04	1.82 ± 0.11	
		0.04	0.04	2.02 ± 0.09	
asym-vc	All tds	0.04	0.04	0.06	
		0.04	0.07	0.05	

Note: For the shortest, mid diastole, and end diastole rows, the ADC_{mean_subjects} and ADC_{SD_subjects} statistics are computed across subjects. For the All tds rows, the ADC_{SD_tds_global} and CV_{tds_global} are statistics are computed across delays by calculating the SD and CV over all trigger delays for each individual subject, then taking a RMS average over all subjects. For the pgse waveform in both kidneys, the ADC_{mean_subjects} is smallest at the shortest trigger delay, which is also true for the asym-vc waveform in the right kidney. In the right kidney, the CV_{tds_global} is similar between pgse and asym-vc for all diffusion directions. In the left kidney, the CV_{tds_global} is similar between pgse and asym-vc for the FH and AP diffusion directions. In the LR direction, asym-vc has a slightly larger CV_{tds_global} than pgse.

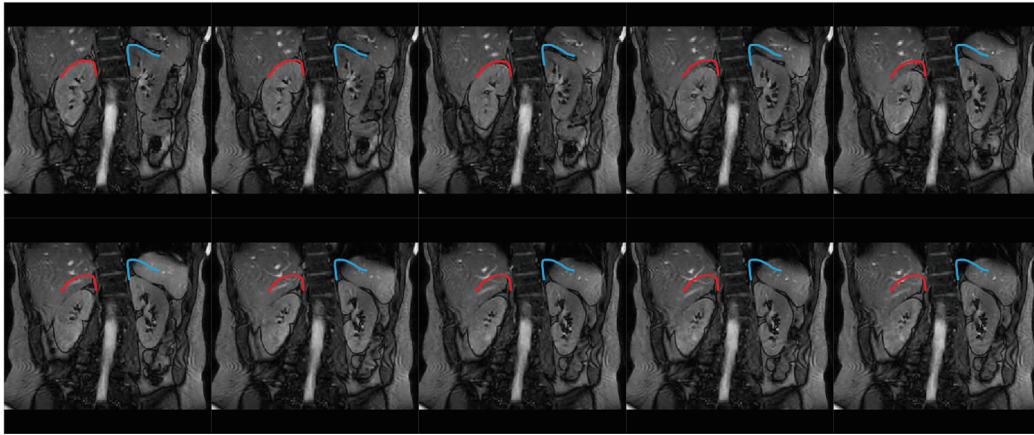


Figure 2 Real-time imaging balanced TFE sequence of the kidneys in the coronal plane in a free breathing scan. Each image is a different frame within the same scan. As guided by the outlines of the top of each kidney (right kidney given in red, left kidney given in blue), both kidneys move a maximum distance on the order of 3 cm as a result of respiratory motion

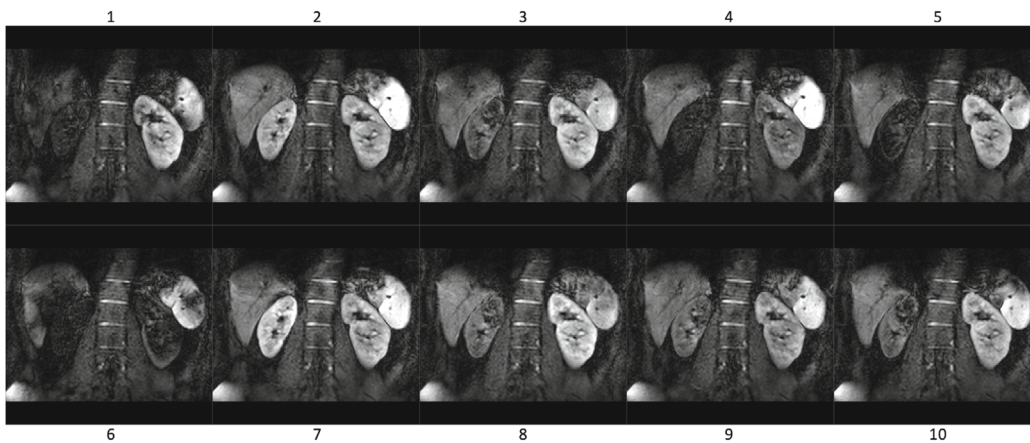


Figure 3 Diffusion weighted ($b = 600 \text{ s/mm}^2$) dynamic scans of the kidney with the pgse diffusion encoding waveform and a respiratory trigger delay of 100 ms, with diffusion being measured in the FH direction. Each image shows different dynamics within the same scan. In many of the dynamics, the right kidney shows a large amount of signal loss as a result of intravoxel dephasing due to motion. The left kidney also shows significant signal loss in some of the dynamics, but not to the same extent as the right kidney

3.4 | Respiratory triggered ADC mapping results

Figure 6 shows individual repetitions of a diffusion weighted ($b = 600 \text{ s/mm}^2$) respiratory triggered (trigger delay = 100 ms) scan for both waveforms with diffusion encoding applied in the LR direction. There is a linear phase across the right side of the body for all repetitions for the pgse waveform, which is likely to be caused by respiratory motion. There is a linear phase variation across the left side of the body, whereas the phase is reasonably constant in the left kidney for all repetitions for the pgse waveform. For the asym-vc waveform, there is some small variation in the phase in the left kidney in the first repetition, but in all other repetitions the phase is reasonably constant in both kidneys.

Figure 7 shows ADC maps for the pgse and asym-vc waveforms at different respiratory trigger delays in two volunteers for diffusion encoding in the FH direction. The ADC in the right kidney in both volunteers at a trigger delay of 100 ms was larger than the corresponding ADC when a trigger delay of 400 ms was used for the pgse waveform. The left kidney also showed a larger ADC at a trigger delay of 100 ms compared to the corresponding ADC at a trigger delay of 400 ms for the pgse waveform in Volunteer 2. The asym-vc waveform showed a more consistent ADC in both of the kidneys between trigger delays in both volunteers in comparison to the pgse waveform.

Figure 8 shows the $\text{ADC}_{\text{mean_subjects}}$ for the FH diffusion direction. For example, in the right kidney of volunteer 9 for the FH diffusion direction, the $\text{ADC}_{\text{mean_subjects}}$ for the pgse waveform were $3.86 \pm 1.07 \times 10^{-3} \text{ mm}^2/\text{s}$,

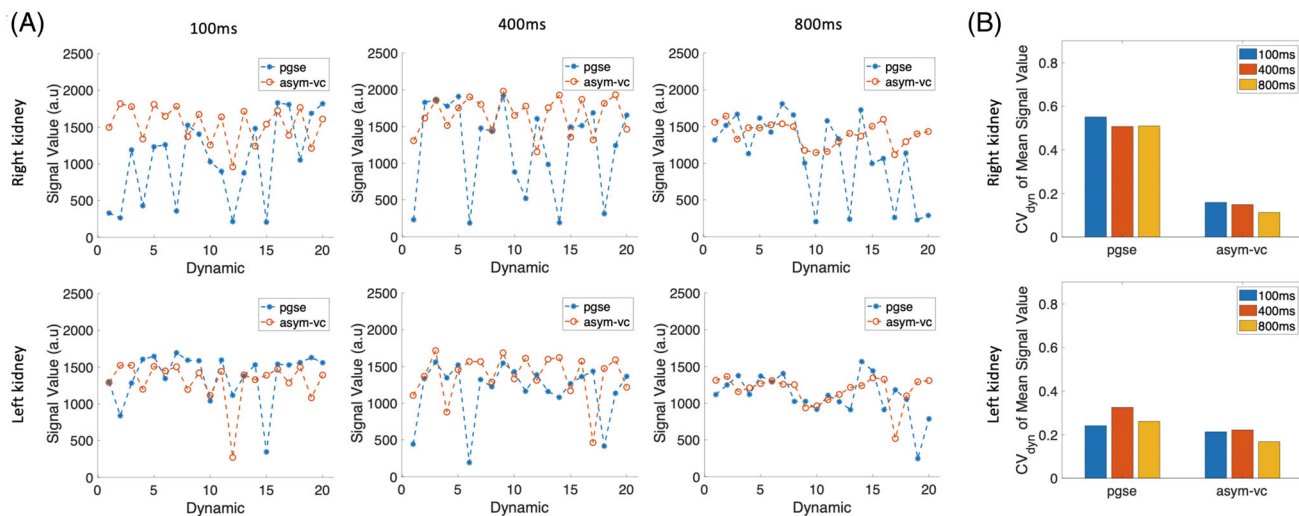


Figure 4 Signal value (A) and CV_{dyn} (B) for the respiratory triggered dynamic scans for diffusion measured in the FH direction in an exemplary subject. In the right kidney, the CV_{dyn} (calculated by measuring the CV over all dynamics) is much larger for all trigger delays for pgse in comparison to asym-vc. It can be seen from the signal value plots in the right kidney that there are many dynamics which exhibit large signal loss when the pgse waveform is used, and that the asym-vc waveform is more stable across dynamics. In the left kidney, the CV_{dyn} of pgse is again larger than that of asym-vc for all trigger delays, but the difference is not as large when compared to the right kidney results

$3.03 \pm 0.72 \times 10^{-3} \text{ mm}^2/\text{s}$, and $2.17 \pm 0.22 \times 10^{-3} \text{ mm}^2/\text{s}$ for the respiratory trigger delays of 100, 400, and 800 ms, respectively; the $ADC_{mean_subjects}$ for the asym-vc waveform were $2.10 \pm 0.17 \times 10^{-3} \text{ mm}^2/\text{s}$, $2.05 \pm 0.26 \times 10^{-3} \text{ mm}^2/\text{s}$, and $2.25 \pm 0.04 \times 10^{-3} \text{ mm}^2/\text{s}$ for the respiratory trigger delays of 100, 400, and 800 ms, respectively. In the right kidney for the FH diffusion direction, the CV_{tds_global} s of pgse and asym-vc were 0.15 and 0.06, respectively. The mean ADCs for all subjects for the LR and AP diffusion directions are shown in the Supporting Information Figures S2 and S3, respectively.

Supporting Information Figure S4 shows the ADC_{mean} s for the FH diffusion direction in the single subject controlled breathing respiratory triggered scan. For example, in the right kidney in the deep breathing case, the ADC_{mean} s for the pgse waveform were $4.06 \pm 0.30 \times 10^{-3} \text{ mm}^2/\text{s}$, $2.81 \pm 0.27 \times 10^{-3} \text{ mm}^2/\text{s}$, and $2.23 \pm 0.15 \times 10^{-3} \text{ mm}^2/\text{s}$ for the respiratory trigger delays of 100, 400, and 800 ms, respectively; the $ADC_{mean_subjects}$ for the asym-vc waveform were $2.25 \pm 0.19 \times 10^{-3} \text{ mm}^2/\text{s}$, $2.14 \pm 0.15 \times 10^{-3} \text{ mm}^2/\text{s}$, and $2.24 \pm 0.22 \times 10^{-3} \text{ mm}^2/\text{s}$ for the respiratory trigger delays of 100, 400, and 800 ms, respectively. In the right kidney in the shallow breathing case, the ADC_{mean} s for the pgse waveform were $2.71 \pm 0.37 \times 10^{-3} \text{ mm}^2/\text{s}$, $2.61 \pm 0.58 \times 10^{-3} \text{ mm}^2/\text{s}$, and $2.04 \pm 0.10 \times 10^{-3} \text{ mm}^2/\text{s}$ for the respiratory trigger delays of 100, 400, and 800 ms, respectively; the $ADC_{mean_subjects}$ for the asym-vc waveform were $2.09 \pm 0.19 \times 10^{-3} \text{ mm}^2/\text{s}$, $2.28 \pm 0.02 \times 10^{-3} \text{ mm}^2/\text{s}$, and $2.15 \pm 0.06 \times 10^{-3} \text{ mm}^2/\text{s}$ for the respiratory trigger delays of 100, 400, and 800 ms, respectively. In the right kidney in the deep breathing case,

the CV_{tds} s of pgse and asym-vc were 0.31 and 0.03, respectively. In the right kidney in the shallow breathing case, the CV_{tds} s of pgse and asym-vc were 0.15 and 0.04, respectively. Supporting Information Figures S5 and S6 show the ADC_{mean} s in the single subject controlled breathing respiratory triggered scan for the LR and AP diffusion directions, respectively.

Table 2 shows the $ADC_{mean_subjects}$, $ADC_{mean_tds_global}$, $ADC_{SD_subjects}$, $ADC_{SD_tds_global}$ and CV_{tds_global} over all subjects for both kidneys. In the right kidney in the FH diffusion direction, pgse had $ADC_{mean_subjects}$ values of $2.45 \pm 0.60 \times 10^{-3} \text{ mm}^2/\text{s}$, $2.22 \pm 0.36 \times 10^{-3} \text{ mm}^2/\text{s}$, and $2.10 \pm 0.26 \times 10^{-3} \text{ mm}^2/\text{s}$ for the respiratory trigger delays of 100, 400, and 800 ms, respectively; the $ADC_{mean_subjects}$ for the asym-vc waveform were $2.14 \pm 0.12 \times 10^{-3} \text{ mm}^2/\text{s}$, $2.10 \pm 0.12 \times 10^{-3} \text{ mm}^2/\text{s}$, and $2.14 \pm 0.12 \times 10^{-3} \text{ mm}^2/\text{s}$ for the respiratory trigger delays of 100, 400, and 800 ms, respectively. In the right kidney for the FH diffusion direction, the CV_{tds_global} s of pgse and asym-vc were 0.15 and 0.06, respectively. In the left kidney for the FH diffusion direction, the CV_{tds_global} s of pgse and asym-vc were 0.07 and 0.05, respectively.

3.5 | SNR mapping scan and simulation results

Supporting Information Figure S7 shows averaged images at $b = 600 \text{ s}/\text{mm}^2$ with ROI apparent SNR values, the predicted relative SNR for the pgse and asym-vc waveforms and a comparison of the increase in TE with increasing

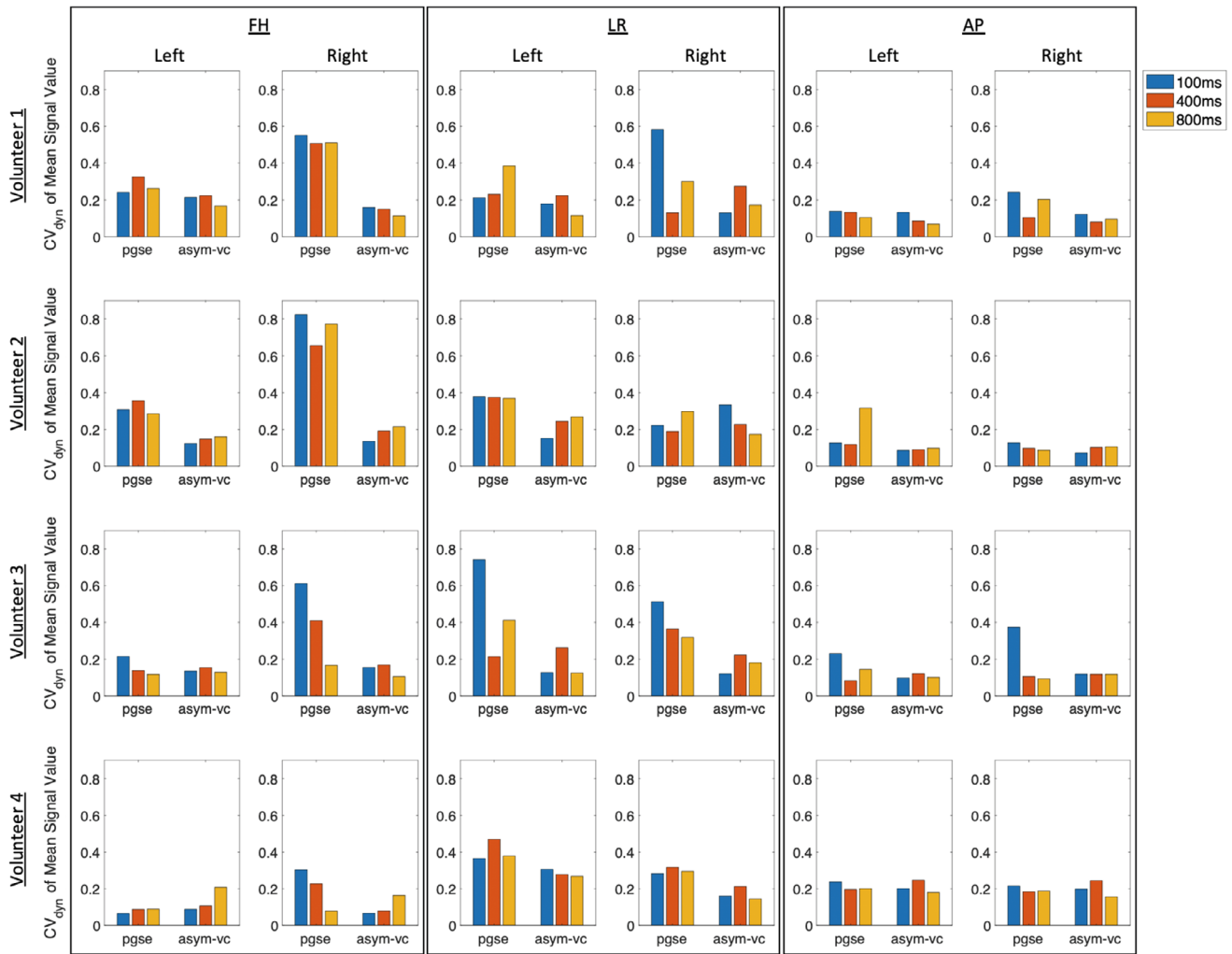


Figure 5 CV_{dyn} (calculated by finding the CV over all dynamics) for all four subjects in the subgroup in which the respiratory triggered dynamic scans were performed. All diffusion directions, both kidneys and all respiratory trigger delays are shown. In general, the largest differences between the CV_{dyn} s of pgse and asym-vc can be seen in the right kidney in the FH diffusion direction, especially at the shortest respiratory trigger delay of 100 ms. pgse also typically has larger CV_{dyn} s than asym-vc in the left kidney, but the differences are not as large as in the right kidney. The FH direction is the direction in which the kidney is expected to move the most during respiration. In all subjects, pgse has a larger CV_{dyn} than asym-vc in the left kidney in the LR diffusion direction at a respiratory trigger delay of 100 ms. In the right kidney in the LR diffusion direction, pgse also typically has a larger CV_{dyn} than asym-vc. Both waveforms have a similar CV_{dyn} in the AP diffusion direction

b -value for both waveforms. The pgse waveform had approximately 20% higher apparent SNR than asym-vc in the left kidney ROI. In comparison, the predicted SNR loss from the extended TE of the asym-vc waveform compared to the pgse waveform at a b -value of 600 s/mm² was approximately 30%.

4 | DISCUSSION

The present work characterizes and assesses motion artifacts in kidney DWI and applies the near TE-optimal motion compensated asym-vc waveform to achieve a more consistent ADC quantification. Respiratory motion

effects are presently shown as an important source of intravoxel signal loss in respiratory triggered DWI scans using pgse waveforms at a short respiratory trigger delay. Despite known disadvantages such as the prolonged TE and reduced SNR, occurrence of bright vessel signal and concomitant effects if asymmetrical waveforms are used, motion-compensated diffusion encoding waveforms remain an alternative approach to motion robust ADC quantification. The asym-vc waveform, or other asymmetric motion-compensated waveforms with similar designs, have, to the best of our knowledge, never been applied in the context of ADC mapping in the kidneys. The presently used near TE-optimal motion compensated asym-vc waveform was able to achieve a more consistent ADC

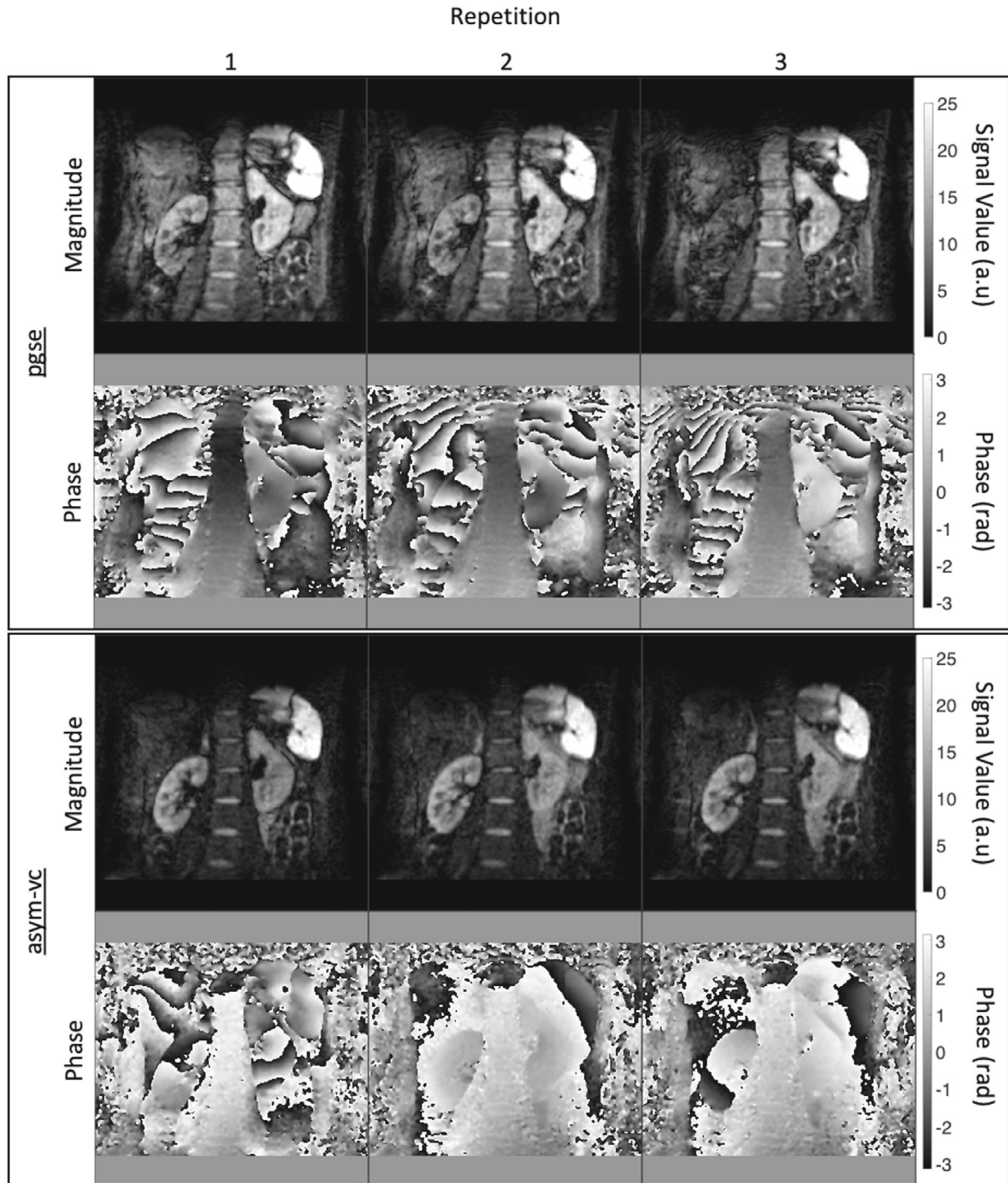


Figure 6 Individual repetitions of a diffusion weighted ($b = 600 \text{ s/mm}^2$) respiratory triggered (trigger delay = 100 ms) scan for both waveforms with diffusion encoding applied in the LR direction. There is a linear phase variation across the right side of the body including the right kidney for all repetitions for the pgse waveform, which is likely to be caused by respiratory motion. The phase is reasonably constant in the left kidney for all repetitions for the pgse waveform. For the asym-vc waveform, there is some small variation in the phase in the left kidney in the first repetition, but in all other repetitions the phase shows less spatial variation in both kidneys

quantification in coronal renal imaging compared to the standard pgse waveform in respiratory triggered DWI scans with a short trigger delay.

The phase images for individual repetitions in a single subject showed a linear phase variation across the entire right side of the body, including within the right kidney

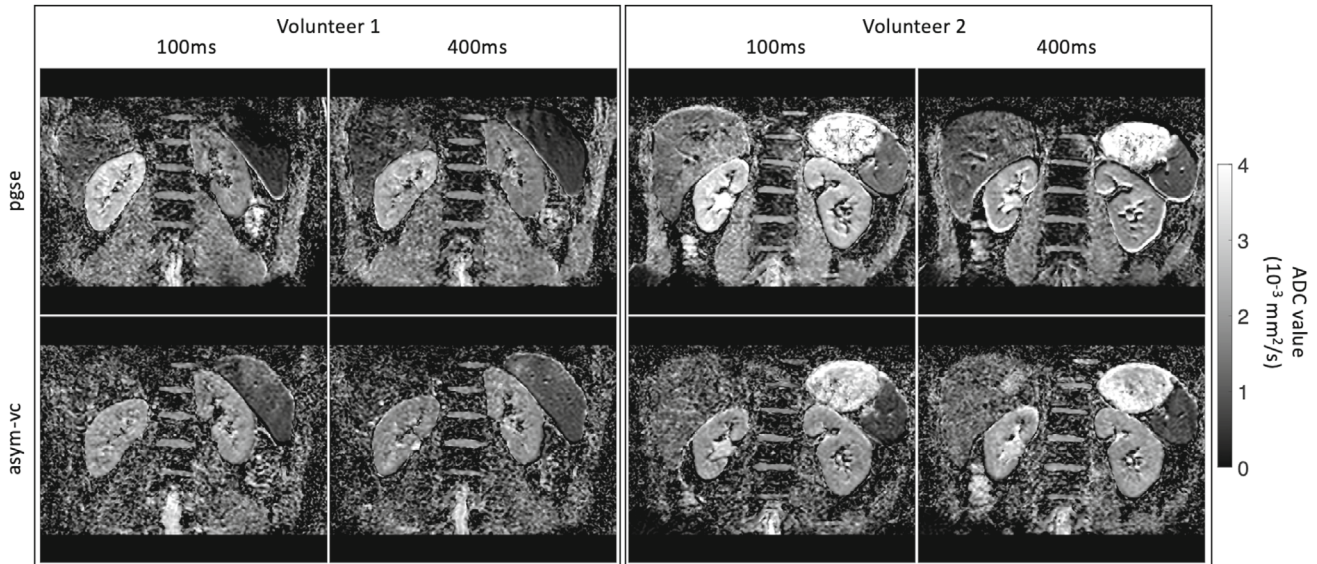


Figure 7 ADC maps for the pgse and asym-vc waveforms at different respiratory trigger delays in two volunteers for diffusion in the FH direction. The ADC in the right kidney in both volunteers at a trigger delay of 100 ms is larger than the corresponding ADC when a trigger delay of 400 ms is used for the pgse waveform. The left kidney also shows a larger ADC at a trigger delay of 100 ms compared to the corresponding ADC at a trigger delay of 400 ms for the pgse waveform in volunteer 2. The asym-vc waveform shows a more consistent ADC in both of the kidneys between trigger delays in both volunteers in comparison to the pgse waveform

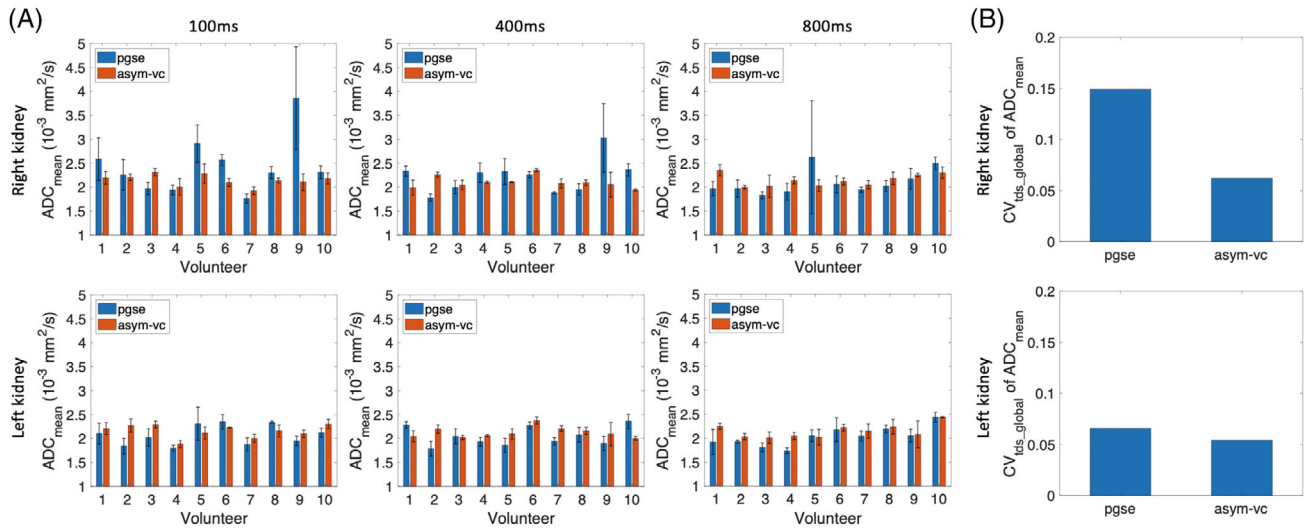


Figure 8 A, ADC_{mean} s (found from averaging over ROIs, then over slices) for all subjects for the FH diffusion direction. The error bars show the SD of the ADCs over slices. At the shortest respiratory trigger delay of 100 ms in the right kidney, there are certain subjects (volunteers 1, 5, 6, and 9) in which there is quite a large variation of ADC across trigger delays for pgse, but not for asym-vc. The differences in mean ADC between pgse and asym-vc are not as large for the longer trigger delays of 400 and 800 ms. B, The CV_{tds_global} (found by calculating the CV over all respiratory trigger delays for each individual subject, then taking a RMS average of all CVs over all subjects) of pgse is much larger than that of asym-vc in the right kidney. In the left kidney, the CV_{tds_global} of pgse is again larger than the CV_{tds_global} of asym-vc, but the difference is not as large as in the right kidney

for the pgse waveform. The linear phase variation suggests that the majority of motion experienced by the kidneys is from respiratory motion, as cardiac motion would be expected to give both more localized and nonlinear phase variation.

The respiratory triggered dynamic scans showed that the kidneys can be affected by intravoxel dephasing due to motion and used a slice thickness of 12 mm, which are relatively thick slices for kidney DWI. A slice thickness of 12 mm was chosen to increase the effect of intravoxel

Table 2 ADC_{mean_subjects}, ADC_{mean_tds_global}, ADC_{SD_subjects}, ADC_{SD_tds_global}, and CV_{tds_global} over all subjects for both kidneys and all diffusion directions across respiratory trigger delays

Kidney	Waveform	Trigger Delay	Diffusion Direction	
			FH	LR
Right kidney	pgse	100 ms	ADC _{mean_subjects} ±	ADC _{mean_subjects} ±
			ADC _{SD_subjects} (10 ⁻³ mm ² /s)	ADC _{SD_subjects} (10 ⁻³ mm ² /s)
			2.45 ± 0.60	2.44 ± 0.60
			2.22 ± 0.36	2.26 ± 0.25
			2.10 ± 0.26	2.14 ± 0.16
			2.14 ± 0.12	2.10 ± 0.35
	asym-vc	400 ms	2.10 ± 0.12	2.19 ± 0.19
			2.14 ± 0.12	2.23 ± 0.20
			ADC _{mean_tds_global} ±	ADC _{mean_tds_global} ±
			ADC _{SD_tds_global} (10 ⁻³ mm ² /s)	ADC _{SD_tds_global} (10 ⁻³ mm ² /s)
pgse	All tds	2.26 ± 0.34	2.28 ± 0.36	
		2.13 ± 0.13	2.17 ± 0.24	
asym-vc	All tds	0.15	0.16	
		0.06	0.11	
Left Kidney	pgse	100 ms	ADC _{mean_subjects} ±	ADC _{mean_subjects} ±
			ADC _{SD_subjects} (10 ⁻³ mm ² /s)	ADC _{SD_subjects} (10 ⁻³ mm ² /s)
			2.07 ± 0.21	2.19 ± 0.16
			2.04 ± 0.20	2.16 ± 0.21
			2.04 ± 0.20	2.17 ± 0.18
			2.15 ± 0.13	2.08 ± 0.32
	asym-vc	400 ms	2.13 ± 0.11	2.19 ± 0.18
			2.15 ± 0.14	2.22 ± 0.21
			ADC _{mean_tds_global} ±	ADC _{mean_tds_global} ±
			ADC _{SD_tds_global} (10 ⁻³ mm ² /s)	ADC _{SD_tds_global} (10 ⁻³ mm ² /s)
pgse	All tds	2.05 ± 0.13	2.17 ± 0.15	
		2.14 ± 0.12	2.16 ± 0.24	
asym-vc	All tds	0.07	0.07	
		0.05	0.11	
Right kidney	pgse	100 ms	ADC _{mean_subjects} ±	ADC _{mean_subjects} ±
			ADC _{SD_subjects} (10 ⁻³ mm ² /s)	ADC _{SD_subjects} (10 ⁻³ mm ² /s)
			2.06 ± 0.31	2.06 ± 0.31
			1.96 ± 0.19	1.96 ± 0.19
			1.89 ± 0.31	1.89 ± 0.31
			2.13 ± 0.19	2.13 ± 0.19
	asym-vc	400 ms	1.96 ± 0.29	1.96 ± 0.29
			2.04 ± 0.13	2.04 ± 0.13
			ADC _{mean_tds_global} ±	ADC _{mean_tds_global} ±
			ADC _{SD_tds_global} (10 ⁻³ mm ² /s)	ADC _{SD_tds_global} (10 ⁻³ mm ² /s)
pgse	All tds	1.97 ± 0.22	1.97 ± 0.22	
		2.04 ± 0.19	2.04 ± 0.19	
asym-vc	All tds	0.11	0.11	
		0.10	0.10	
Left Kidney	pgse	100 ms	ADC _{mean_subjects} ±	ADC _{mean_subjects} ±
			ADC _{SD_subjects} (10 ⁻³ mm ² /s)	ADC _{SD_subjects} (10 ⁻³ mm ² /s)
			1.88 ± 0.11	1.88 ± 0.11
			1.87 ± 0.16	1.87 ± 0.16
			1.90 ± 0.32	1.90 ± 0.32
			2.06 ± 0.18	2.06 ± 0.18
	asym-vc	400 ms	1.93 ± 0.29	1.93 ± 0.29
			1.99 ± 0.11	1.99 ± 0.11
			ADC _{mean_tds_global} ±	ADC _{mean_tds_global} ±
			ADC _{SD_tds_global} (10 ⁻³ mm ² /s)	ADC _{SD_tds_global} (10 ⁻³ mm ² /s)
pgse	All tds	1.88 ± 0.18	1.88 ± 0.18	
		1.99 ± 0.17	1.99 ± 0.17	
asym-vc	All tds	0.10	0.10	
		0.09	0.09	

Note: For the 100, 400, and 800 ms delay rows, the ADC_{mean_subjects} and ADC_{SD_subjects} statistics are computed across subjects. For the All tds rows, the ADC_{SD_tds_global} and CV_{tds_global} are statistics are computed across delays by calculating the SD and CV over all trigger delays for each individual subject, then taking a RMS average over all subjects. In the right kidney for the FH diffusion direction, the ADC_{mean_subjects} of pgse is largest at a respiratory trigger delay of 100 ms, and decreases as the respiratory trigger delay increases. The same trend exists for the ADC_{SD_subjects}·pgse has a larger CV_{tds_global} than asym-vc in the right kidney in the FH and LR diffusion directions. The CV_{tds_global}s for pgse and asym-vc are approximately the same in the AP diffusion direction in the right kidney. In the left kidney, the ADC_{mean_subjects} are more consistent across trigger delays for both waveforms than in the right kidney. Overall, the range of ADC_{mean_subjects} values between trigger delays is larger for pgse than for asym-vc in the right kidney, and the left kidney does not appear to be as affected by motion as the right kidney.

dephasing and, therefore, to more clearly highlight the signal stability for each waveform, kidney, diffusion direction, and respiratory trigger delay.

In the respiratory triggered ADC mapping scans with a 6 mm slice thickness (Figures 7 and 8), there were higher ADC values at shorter trigger delays compared to longer trigger delays. In the right kidney for the pgse waveform, there were certain volunteers which had an ADC that decreased as the trigger delay increased, again suggesting that respiratory motion is the main cause of signal loss in the kidneys. The ADC values of certain volunteers were not as affected by motion, which could be a result of how quickly or deeply the subject breathes, or also whether the subject breathes more with the belly or chest, which leads to different degrees of diaphragm motion. Table 2 showed the $ADC_{\text{mean_subjects}}$, $ADC_{\text{mean_tds_global}}$, $ADC_{\text{SD_subjects}}$, $ADC_{\text{SD_tds_global}}$, and $CV_{\text{tds_global}}$ over all volunteers for all diffusion directions and both kidneys. The range of $ADC_{\text{mean_subjects}}$ between trigger delays was larger in the respiratory triggered scans than the breath held cardiac triggered scans (shown in Table 1), and the $ADC_{\text{SD_subjects}}$ of the respiratory triggered scans for the pgse waveform at short respiratory trigger delays were generally larger than the $ADC_{\text{SD_subjects}}$ of the breath-held cardiac triggered scans, suggesting that respiratory motion affects the kidney much more than cardiac motion. The asym-vc waveform was able to reduce the range of $ADC_{\text{mean_subjects}}$ between trigger delays in the FH and LR diffusion directions in the right kidney compared to pgse, suggesting good performance of the motion compensating capabilities of the asym-vc waveform. It is not immediately clear why the right kidney would be more affected than the left kidney and would require further investigation.

The single subject controlled breathing respiratory triggered ADC mapping results (shown in the Supporting Information Figures S4 to S6) showed that there was a larger variation in the ADC_{mean} s between different trigger delays in the FH diffusion direction for the pgse waveform in the deep breathing case in comparison to the shallow breathing case, which is further evidence that the majority of motion induced signal loss in the kidneys is caused primarily by respiratory motion rather than cardiac motion.

The asym-vc waveform has a prolonged TE in comparison to the pgse waveform, which causes a reduction in SNR. In the in vivo averaged images shown in Supporting Information Figure S7(a), both waveforms had adequate SNR, and both waveforms had bright regions in their respective SNR maps which could have been caused by residual vessel signal. Despite the controlled shallow breathing of the volunteer and a respiratory trigger delay of 800 ms, motion effects could still be present at a b -value of 600 s/mm^2 , which is why the experimentally

determined SNR values were labeled presently as apparent SNR values.

Previous works have suggested that renal blood flow is pulsatile and depends on the cardiac cycle, which affects the perfusion fraction [13]. Some recent studies have also proposed a dependence of the ADC on the cardiac cycle, while however using low b -values ($b < 50 \text{ s/mm}^2$) in the ADC extraction [8,10,12]. However, using low b -values and a monoexponential diffusion expression can transfer the cardiac cycle dependence of the perfusion fraction to the ADC extraction [13]. Another study using both low and high b -values and modeling both diffusion and perfusion effects showed better reproducibility of the DW signal for respiratory-cardiac double-triggering compared to only respiratory triggering [11]. The present results show that respiratory motion can be a major source of signal loss in respiratory-triggered pgse scans with short trigger delays and diffusion encoding in the FH direction. Cardiac triggering might be able to further improve reproducibility of respiratory-triggered pgse scans with long respiratory trigger delays; however, the presented results suggest that the impact of cardiac motion on ADC quantification can be smaller compared to respiratory motion effects at short respiratory trigger delays, at least in the b -value range used. In Binser et al [11], there was a larger variability in the mean ADC values for the (navigator based) respiratory triggered scans compared to the double cardiac and respiratory triggered scans; however the difference in mean ADC values between the respiratory and double triggered scans was small and not statistically significant, which is in agreement with our presented results. In Kataoka et al [9], only small differences were observed between respiratory triggered and breath-held sequences. However, smaller b -values were used, potentially reducing the effect of motion on ADC quantification. Previous works have measured the displacement of the kidneys during respiration. In Moerland et al [48], there were considerable variations in the FH displacement in forced respiration and normal respiration scans, both between subjects and in some cases between the right and left kidneys. On average, the right kidney had a larger displacement than the left kidney. A larger displacement of one kidney relative to the other can explain why the ADC values could differ between kidneys for a given diffusion direction. In Brandner et al [49], the displacement of the kidneys was measured in 3D. The 2D graphs of the AP displacement relative to the FH displacement for each patient and kidney at different parts of the breathing cycle showed that the motion is complex and differs between subjects. A review paper from Pham et al [50] compared studies measuring kidney displacements in the FH, LR, and AP directions under different breathing conditions. In the context of DWI, it is the motion during diffusion encoding rather than the

absolute displacement during the whole respiratory cycle that causes signal loss, and is also likely to be complex and vary considerably between subjects.

The present work has some limitations. First, only 10 volunteers were scanned, with two different subsets of only 4 volunteers each for the respiratory triggered dynamic scans and the breath held cardiac triggered scans. The respiratory triggered dynamic scans and the breath held cardiac triggered scans were split into two different subgroups to avoid excessively long total scan times. Further work would be required to fully characterize the effect of cardiac motion on the kidneys, and to fully assess what role the breathing pattern of each individual plays in the ADC quantification of the kidneys at different parts of the breathing cycle, especially in patients. Second, separate ROIs were not drawn for the cortex and the medulla, due to the difficulty of accurately drawing ROIs in the cortex and medulla when there is slice misalignment. In the present work where respiratory motion is expected, slice misalignment is more likely. Third, a respiratory belt was used to track respiratory motion. If the respiratory belt is not positioned correctly, or the signal received from the respiratory belt is noisy, the triggering of the sequence may not be accurate. Due to individual differences in breathing patterns, a longer trigger delay is not necessarily less affected by motion than a shorter trigger delay, and irregular breathing patterns can cause motion artifacts regardless of the trigger delay. Fourth, the present work used DWI data acquired at two b -values and three diffusion directions and thus did not model perfusion effects and diffusion anisotropy effects. Therefore, the present results could not be directly translated to the effect of motion on the robustness of intravoxel incoherent motion (IVIM) and DTI parameter extraction. Fifth, use of the lower b -value of 100 s/mm^2 was chosen to reduce the effect of perfusion [51] without sensitizing the signal too much to motion effects. However, it is possible that some perfusion signal remained, which can confound the results for the ADC values for both waveforms. The upper b -value of 600 s/mm^2 was chosen to find the balance between diffusion contrast and adequate SNR. Finally, the use of the motion compensated diffusion encoding waveforms reduces the sensitivity to motion at the cost of reduced SNR. Therefore, if the SNR of the DWI scan is already low (e.g., due to high b -value or high spatial-resolution), motion compensated diffusion encoding waveforms might not be preferable to avoid any noise-induced bias in the ADC quantification.

5 | CONCLUSIONS

Respiratory and cardiac motion effects were characterized and assessed in the context of kidney DWI, where

the near TE-optimized motion compensated asym-vc diffusion encoding waveform was compared with the standard pgse diffusion encoding waveform. The breath held cardiac triggered results showed that neither kidney was largely affected by cardiac motion. The respiratory triggered ADC mapping results showed that the right kidney is more affected than the left kidney by respiratory motion in the FH and LR diffusion directions when the pgse diffusion encoding waveform is used, and that the asym-vc was able to reduce the ADC quantification errors caused by respiratory motion at the cost of reduced SNR.


ACKNOWLEDGMENTS

The present work was supported by Philips Healthcare. Open Access funding enabled and organized by Projekt DEAL. Open Access funding enabled and organized by Projekt DEAL.

CONFLICT OF INTEREST

Johannes M. Peeters and Kilian Weiss are employees of Philips Healthcare. Dimitrios C. Karampinos receives grant support from Philips Healthcare.

ORCID

Sean McTavish  <https://orcid.org/0000-0003-4788-6526>

REFERENCES

1. Zhao J, Wang ZJ, Liu M, et al. Assessment of renal fibrosis in chronic kidney disease using diffusion-weighted MRI. *Clin Radiol*. 2014;69:1117-1122.
2. Damasio MB, Tagliafico A, Capaccio E, et al. Diffusion-weighted MRI sequences (DW-MRI) of the kidney: normal findings, influence of hydration state and repeatability of results. *Radiol Med*. 2008;113:214-224.
3. Zhang JL, Sigmund EE, Chandarana H, et al. Variability of renal apparent diffusion coefficients: limitations of the Monoexponential model for diffusion quantification. *Radiology*. 2010;254:783-792.
4. Li Q, Li J, Zhang L, Chen Y, Zhang M, Yan F. Diffusion-weighted imaging in assessing renal pathology of chronic kidney disease: a preliminary clinical study. *Eur J Radiol*. 2014;83:756-762.
5. Kline TL, Edwards ME, Garg I, et al. Quantitative MRI of kidneys in renal disease. *Abdom Radiol (NY)*. 2018;43:629-638.
6. Namimoto T, Yamashita Y, Mitsuzaki K, Nakayama Y, Tang Y, Takahashi M. Measurement of the apparent diffusion coefficient in diffuse renal disease by diffusion-weighted echo-planar MR imaging. *J Magn Reson Imaging*. 1999;9:832-837.
7. Ljimini A, Caroli A, Laustsen C, et al. Consensus-based technical recommendations for clinical translation of renal diffusion-weighted MRI. *Magma*. 2020;33:177-195.
8. Heusch P, Wittsack HJ, Kröppel P, et al. Impact of blood flow on diffusion coefficients of the human kidney: a time-resolved ECG-triggered diffusion-tensor imaging (DTI) study at 3T. *J Magn Reson Imaging*. 2013;37:233-236.
9. Kataoka M, Kido A, Yamamoto A, et al. Diffusion tensor imaging of kidneys with respiratory triggering: optimization of

- parameters to demonstrate anisotropic structures on fraction anisotropy maps. *J Magn Reson Imaging*. 2009;29:736-744.
10. Ito K, Hayashida M, Kanki A, et al. Alterations in apparent diffusion coefficient values of the kidney during the cardiac cycle: evaluation with ECG-triggered diffusion-weighted MR imaging. *Magn Reson Imaging*. 2018;52:1-8.
 11. Binser T, Thoeny HC, Eisenberger U, Stemmer A, Boesch C, Vermathen P. Comparison of physiological triggering schemes for diffusion-weighted magnetic resonance imaging in kidneys. *J Magn Reson Imaging*. 2010;31:1144-1150.
 12. Lanzman RS, Ljimini A, Müller-Lutz A, et al. Assessment of time-resolved renal diffusion parameters over the entire cardiac cycle. *Magn Reson Imaging*. 2019;55:1-6.
 13. Wittsack HJ, Lanzman RS, Quentin M, et al. Temporally resolved electrocardiogram-triggered diffusion-weighted imaging of the human kidney: correlation between intravoxel incoherent motion parameters and renal blood flow at different time points of the cardiac cycle. *Invest Radiol*. 2012;47:226-230.
 14. Stejskal EO, Tanner JE. Spin diffusion measurements: spin echoes in the presence of a time-dependent field gradient. *J Chem Phys*. 1965;42:288-292.
 15. Caroli A, Schneider M, Friedli I, et al. Diffusion-weighted magnetic resonance imaging to assess diffuse renal pathology: a systematic review and statement paper. *Nephrol Dial Transplant*. 2018;33:ii29-ii40.
 16. Squillaci E, Manenti G, Cova M, et al. Correlation of diffusion-weighted MR imaging with cellularity of renal Tumours. *Anticancer Res*. 2004;24:4175-4180.
 17. Wang HY, Wang J, Tang YH, Ye HY, Ma L. Coronal diffusion-weighted magnetic resonance imaging of the kidney: agreement with axial diffusion-weighted magnetic imaging in terms of apparent diffusion coefficient values. *Chin Med J (Engl)*. 2015;128:499-503.
 18. Wang WJ, Pui MH, Guo Y, Hu XS, Wang HJ, Yang D. MR diffusion tensor imaging of normal kidneys. *J Magn Reson Imaging*. 2014;40:1099-1102.
 19. Bruegel M, Holzapfel K, Gaa J, et al. Characterization of focal liver lesions by ADC measurements using a respiratory triggered diffusion-weighted single-shot echo-planar MR imaging technique. *Eur Radiol*. 2008;18:477-485.
 20. Gourtsoyianni S, Papanikolaou N, Yarmenitis S, Maris T, Karantanis A, Gourtsoyiannis N. Respiratory gated diffusion-weighted imaging of the liver: value of apparent diffusion coefficient measurements in the differentiation between most commonly encountered benign and malignant focal liver lesions. *Eur Radiol*. 2008;18:486-492.
 21. Kwee TC, Takahara T, Koh DM, Nievelstein RA, Luijten PR. Comparison and reproducibility of ADC measurements in breathhold, respiratory triggered, and free-breathing diffusion-weighted MR imaging of the liver. *J Magn Reson Imaging*. 2008;28:1141-1148.
 22. Kwee TC, Takahara T, Niwa T, et al. Influence of cardiac motion on diffusion-weighted magnetic resonance imaging of the liver. *Magma*. 2009;22:319-325.
 23. Murphy P, Wolfson T, Gamst A, Sirlin C, Bydder M. Error model for reduction of cardiac and respiratory motion effects in quantitative liver DW-MRI. *Magn Reson Med*. 2013;70:1460-1469.
 24. Taouli B, Sandberg A, Stemmer A, et al. Diffusion-weighted imaging of the liver: comparison of navigator triggered and breathhold acquisitions. *J Magn Reson Imaging*. 2009;30:561-568.
 25. Hahn S, Absil J, Debeir O, Metens T. Assessment of cardiac-driven liver movements with filtered harmonic phase image representation, optical flow quantification, and motion amplification. *Magn Reson Med*. 2019;81:2788-2798.
 26. Metens T, Absil J, Denolin V, Bali MA, Matos C. Liver apparent diffusion coefficient repeatability with individually predetermined optimal cardiac timing and artifact elimination by signal filtering. *J Magn Reson Imaging*. 2016;43:1100-1110.
 27. Rauh SS, Riexinger AJ, Ohlmeyer S, et al. A mixed waveform protocol for reduction of the cardiac motion artifact in black-blood diffusion-weighted imaging of the liver. *Magn Reson Imaging*. 2020;67:59-68.
 28. Aliotta E, Wu HH, Ennis DB. Convex optimized diffusion encoding (CODE) gradient waveforms for minimum echo time and bulk motion compensated diffusion weighted MRI. *Magn Reson Med*. 2017;77:717-729.
 29. Szczepankiewicz F, Sjölund J, Dall'Armellina E, et al. Motion-compensated gradient waveforms for tensor-values diffusion encoding by constrained numerical optimization. *Magn Reson Med*. 2021;85:2117-2126.
 30. Lasič S, Szczepankiewicz F, Dall'Armellina E, et al. Motion-compensated b-tensor encoding for in vivo cardiac diffusion-weighted imaging. *NMR Biomed*. 2020;33:e4213.
 31. Dou J, Reese TG, Tseng WY, Wedeen VJ. Cardiac diffusion MRI without motion effects. *Magn Reson Med*. 2002;48:105-114.
 32. Stoeck CT, von Deuster C, Genet M, Atkinson D, Kozerke S. Second-order motion-compensated spin echo diffusion tensor imaging of the human heart. *Magn Reson Med*. 2016;75:1669-1676.
 33. Majeed W, Kalra P, Kolipaka A (2018) Motion Compensated, Optimized Diffusion Encoding (MODE) Gradient Waveforms. In: Proceedings of the 26th Annual Meeting of ISMRM.: Abstract 1614.
 34. McTavish S, Van AT, Peeters J, Ogino T, Hock A, Rummeny E, Braren R, Karampinos DC (2019) Partial velocity-compensated optimized diffusion encoding for combined motion compensation and residual vessel signal suppression in liver ADC mapping. In: Proceedings of the 27th Annual Meeting of ISMRM. Montréal, Canada: Abstract 1709.
 35. McTavish S, Van AT, Peeters JM, Weiss K, Makowski MR, Braren RF, Karampinos DC (2021) Gradient nonlinearity correction in liver DWI using motion-compensated diffusion encoding waveforms. *Magma*. 2021; doi: 10.1007/s10334-021-00981-6
 36. Ozaki M, Inoue Y, Miyati T, et al. Motion artifact reduction of diffusion-weighted MRI of the liver: use of velocity-compensated diffusion gradients combined with tetrahedral gradients. *J Magn Reson Imaging*. 2013;37:172-178.
 37. Peña-Nogales Ó, Zhang Y, Wang X, et al. Optimized diffusion-weighting gradient waveform design (ODGD) formulation for motion compensation and concomitant gradient nulling. *Magn Reson Med*. 2019;81:989-1003.
 38. Van AT, Cervantes B, Ogino T, Peeters JM, Hock A, Rummeny EJ, Braren R, Karampinos DC (2018) Partial velocity-compensated diffusion encoding for combined motion compensation and residual vessel signal suppression in liver DWI. In: Proceedings of the 26th Annual Meeting of ISMRM. Paris, France: Abstract 0079.

39. Zhang Y, Peña-Nogales Ó, Holmes JH, Hernando D. Motion-robust and blood suppressed M1-optimized diffusion MR imaging of the liver. *Magn Reson Med*. 2019;82:302-311.
40. Geng R, Zhang Y, Starekova J, et al. Characterization and correction of cardiovascular motion artifacts in diffusion-weighted imaging of the pancreas. *Magn Reson Med*. 2021;86:1956-1969.
41. Sjölund J, Szczepankiewicz F, Nilsson M, Topgaard D, Westin CF, Knutsson H. Constrained optimization of gradient waveforms for generalized diffusion encoding. *J Magn Reson*. 2015;261:157-168.
42. Szczepankiewicz F, Eichner C, Anwander A, Westin CF, Paquette M (2020) The impact of gradient non-linearity on Maxwell compensation when using asymmetric gradient waveforms for tensor-valued diffusion encoding. In: Proceedings of the 28th Annual Meeting of ISMRM. Abstract 3391.
43. Szczepankiewicz F, Sjölund J. Cross-term-compensated gradient waveform design for tensor-values diffusion MRI. *J Magn Reson*. 2021;328:106991. doi:10.1016/j.jmr.2021.106991
44. Szczepankiewicz F, Westin CF, Nilsson M. Maxwell-compensated design of asymmetric gradient waveforms for tensor-valued diffusion encoding. *Magn Reson Med*. 2019;82:1424-1437.
45. Storey P, Frigo FJ, Hinks RS, et al. Partial k-space reconstruction in single-shot diffusion-weighted echo-planar imaging. *Magn Reson Med*. 2007;57:614-619.
46. Van AT, McTavish S, Peeters JM, Weiss K, Makowski MR, Braren RF, Karampinos DC (2021) Phase correction in liver single-shot DW-EPI acquired with partial Fourier encoding. In: Proceedings of the 29th Annual Meeting of ISMRM. Virtual Conference: Abstract 2129.
47. Weingärtner S, Desmond KL, Obuchowski NA, et al. Development, validation, qualification, and dissemination of quantitative MR methods: overview and recommendations by the ISMRM quantitative MR study group. *Magn Reson Med*. 2022;87:1184-1206.
48. Moerland MA, van den Bergh AC, Bhagwandien R, et al. The influence of respiration induced motion of the kidneys on the accuracy of radiotherapy treatment planning, a magnetic resonance imaging study. *Radiother Oncol*. 1994;30:150-154.
49. Brandner ED, Wu A, Chen H, et al. Abdominal organ motion measured using 4D CT. *Int J Radiation Oncology Biol Phys*. 2006;65:554-560.
50. Pham D, Kron T, Foroudi F, Schneider M, Siva S. A review of kidney motion under free, deep and forced-shallow breathing conditions: implications for stereotactic ablative body radiotherapy treatment. *Technol Cancer Res Treat*. 2014;13:315-323.
51. Wurnig MC, Donati OF, Ulbrich E, et al. Systematic analysis of the intravoxel incoherent motion threshold separating perfusion and diffusion effects: proposal of a standardized algorithm. *Magn Reson Med*. 2015;74:1414-1422.

SUPPORTING INFORMATION

Additional supporting information may be found in the online version of the article at the publisher's website.

Figure S1 ADC_{mean} s for the breath held cardiac triggered ADC mapping scans, for the full subset of 4 subjects, for both kidneys and for all measured diffusion directions.

In general, the shortest cardiac trigger delay gives slightly smaller ADC values than the mid diastole and end diastole cardiac trigger delays. The difference is, however, small. There is no significant observable trend between the cardiac trigger delays or waveforms

Figure S2 ADC_{mean} s (a) (found from averaging over ROIs, then over slices) for all subjects for the LR diffusion direction. The error bars show the standard deviation of the ADCs over slices. At the shortest respiratory trigger delay of 100 ms in the right kidney, there are certain subjects (volunteers 2, 6 and 9) in which the ADC shows a large variation across trigger delays for pgse, but the asym-vc waveform does not show as large of a variation in ADC across trigger delays. The differences in mean ADC between pgse and asym-vc are not as large for the longer trigger delays of 400 and 800 ms. Also shown is the $CV_{\text{tds_global}}$ (b)

Figure S3 ADC_{mean} s (a) (found from averaging over ROIs, then over slices) for all subjects for the AP diffusion direction. The error bars show the standard deviation of the ADCs over slices. The differences in mean ADC between pgse and asym-vc are not large for any of the respiratory trigger delays except for outliers. Also shown is the $CV_{\text{tds_global}}$ (b)

Figure S4 ADC_{mean} s (a) (determined by averaging over ROIs, then over slices) for the FH diffusion direction in a single subject under three different breathing patterns (deep, medium and shallow). Also shown is the CV_{td} (b), determined by calculating the CV over all trigger delays, for each breathing pattern – deep, medium and shallow. The pgse waveform has an ADC_{mean} that varies by a large amount between trigger delays for the deep and medium breathing patterns for both the left and right kidneys. The asym-vc has a more consistent ADC_{mean} over trigger delays for both kidneys for all breathing patterns, as highlighted by the lower CV_{td} s in all cases

Figure S5 ADC_{mean} s (a) (determined by averaging over ROIs, then over slices) for the LR diffusion direction in a single subject under three different breathing patterns (deep, medium and shallow). Also shown is the CV_{td} (b), determined by calculating the CV over all trigger delays, for each breathing pattern – deep, medium and shallow. The pgse waveform has an ADC_{mean} that varies by a large amount between trigger delays for the deep and medium breathing patterns for the left kidney, and an ADC_{mean} that varies by a moderate amount between trigger delays for the deep and medium breathing patterns for the right kidney. The asym-vc has a more consistent ADC_{mean} over trigger delays for both kidneys for the deep and medium breathing patterns, as highlighted by the lower CV_{td} s for those breathing patterns

Figure S6 ADC_{mean} s (a) (determined by averaging over ROIs, then over slices) for the AP diffusion direction in

a single subject under three different breathing patterns (deep, medium and shallow). Also shown is the CV_{td} (b), determined by calculating the CV over all trigger delays, for each breathing pattern – deep, medium and shallow. The pgse waveform has an ADC_{mean} that is mostly stable between trigger delays for the medium and shallow breathing patterns for both kidneys, with the largest ADC_{mean} values coming from the cases with deep breathing and a respiratory trigger delay of 100 ms. The asym-vc has a reasonably consistent ADC_{mean} over trigger delays for both kidneys for all breathing patterns

Figure S7 Shown in (a) are diffusion-weighted images found from averaging over 3 repetitions in a controlled shallow breathing respiratory triggered scan with a respiratory trigger delay of 800 ms. The apparent SNR values (using difference images) over the ROIs are also shown in red. The b -value used was 600 s/mm^2 , meaning that motion effects may affect the apparent SNR values. Both waveforms have regions of high apparent SNR that may be caused by residual vessel signal. In the ROI in the left kidney, pgse has approximately 20% higher apparent SNR than asym-vc. The asym-vc waveform, however, still has adequate apparent SNR. By comparison, the

difference in the apparent SNR between pgse and asym-vc is much higher in the liver, where the signal of the liver is close to the noise floor when using the asym-vc waveform. Shown in (b) is the theoretically predicted relative SNR for different b -values, determined by considering the echo times from the scanner at different b -values and predicting the SNR relative to the $b = 0 \text{ s/mm}^2$ acquisition. At a b -value of 600 s/mm^2 , as used in the respiratory triggered ADC mapping, the expected reduction of SNR for the asym-vc waveform compared to the pgse waveform is approximately 30%, and is thus a similar order of magnitude to the experimental results. Shown in (c) are the echo times for each waveform for a range of b -values. As the b -value increases, the difference in TE between the two waveforms gets larger

How to cite this article: McTavish S, Van AT, Peeters JM, et al. Motion compensated renal diffusion weighted imaging. *Magn Reson Med.* 2023;89:144-160. doi: 10.1002/mrm.29433